Probing the Environment of Cu_B in Heme−Copper Oxidases

Vangelis Daskalakis,[†] Eftychia Pinakoulaki,[‡] Stavros Stavrakis,[†] and Constantinos Varotsis*,[†]

Department of Chemistry, University of Crete, 71003 Voutes, Heraklion, Crete, Greece, and Department of Chemistry, University of Cyprus, P.O. Box 20537, 1678 Nicosia, Cyprus

Received: March 7, 2007; In Final Form: June 10, 2007

Time-resolved step-scan FTIR (TRS^2-FTIR) and density functional theory have been applied to probe the structural dynamics of Cu_B in heme−copper oxidases at room temperature. The TRS^2-FTIR data of cbb_3 from *Pseudomonas stutzeri* indicate a small variation in the frequency of the transient CO bound to Cu_B in the pH/pD 7−9 range. This observation in conjunction with density functional theory calculations, in which significant frequency shifts of the ν(CO) are observed upon deprotonation and/or detachment of the Cu_B ligands, demonstrates that the properties of the Cu_B ligands including the cross-linked tyrosine, in contrast to previous reports, remain unchanged in the pH 7−9 range. We attribute the small variations in the ν(CO) of Cu_B to protein conformational changes in the vicinity of Cu_B. Consequently, the split of the heme Fe−CO vibrations (α-, β-, and γ-forms) is not due to changes in the ligation and/or protonation states of the Cu_B ligands or to the presence of one or more ionizable groups, as previously suggested, but the result of global protein conformational changes in the vicinity of Cu_B which, in turn, affect the position of Cu_B with respect to the heme Fe.

Cytochrome *c* oxidase (CcO) is an integral membrane enzyme of the respiratory chain which contains a homo−dinuclear Cu_A center, one low-spin heme *a*, and a high-spin heme a_3−Cu_B binuclear center where the reduction of dioxygen to H_2O takes place.[1−6] The dioxygen reaction is coupled to the translocation of protons across the lipid bilayer, creating a pH and voltage gradient across the membrane.[1] Consequently, there are groups in the protein that are redox sensitive and undergo protonation/deprotonation events associated with the functional processes in the enzyme. One of the unique properties of the binuclear heme a_3−Cu_B center that was determined by the crystal structures of the bovine, the *Paracoccus denitrificans*, and the *Thermus thermophilus* heme−copper oxidases is the Y280-His276 (*P. denitrificans* numbering) cross-linked structure.[7−9] Y280 is located at the end of the proton K-channel and is highly conserved among the heme−copper oxidases. A wealth of information is available on the functional properties of the protonation/deprotonation events of groups near the catalytic center that may play or not essential roles in the delivery of protons for the dioxygen reduction chemistry and proton pumping.[10−13] On this line, several model complexes have also been synthesized to mimic the binuclear center and to determine the pK_a of the cross-linked tyrosine.[14−18] Accordingly, the protonation/deprotonation events at the binuclear center coupled to the dynamics and chemistry occurring at the heme−Fe is crucial in elucidating the functional properties of the enzyme.

It has been suggested that the major conformations (α and β) at the binuclear center and the existence of equilibrium between them might have significant importance in the enzymatic activity of heme−copper oxidases.[19−27] For instance, in certain mutant heme−copper oxidases, low-frequency Fe−CO stretching modes were detected (β-form), and the enzyme had no dioxygen reduction activity.[20,23] However, due to the presence of both forms the activity of the population with the β-form could not be determined. The α- and β-conformational states of heme−copper oxidases, although their functional significance and the origin for the splitting have not been established, have been attributed to changes in the distance between the iron atom of heme a_3 and Cu_B and the existence of both a H- and a non-H-bonded proximal heme Fe−His ligand.[10,19,22,24−29] On this line, it was postulated that the different structures result from a change in the position of the Cu_B atom with respect to the Fe−CO due to the presence of one or more ionizable groups.[19,24,25] Possible candidates included the cross-linked, conserved tyrosine that is adjacent to the oxygen-binding pocket or one of the histidines that coordinates to Cu_B. On the other hand, it has been reported that the α/β ratio at a given pH was altered by point mutations in the vicinity of the binuclear center suggesting that local changes on polarity sensed at the binuclear center may be coupled to a more global protein conformational change.[20]

Three distinct families of heme−copper oxidases have been identified. The type-A oxidase superfamily is similar to the mitochondrial (aa_3) enzyme.[1] The type-B oxidase is related to the ba_3 from *T. thermophilus*, whereas the type-C are the cbb_3-type oxidases.[9,30−34,40] The thermophilic Gram-negative eubacterium *T. thermophilus* HB8 (ATCC27634) expresses cytochromes caa_3 and ba_3 that serve as terminal oxidases for reducing oxygen to water.[9] A comparative study of ba_3 and caa_3 has shown that fully active heme−copper oxidases can have binuclear centers in which either the α- or the β-form is present.[24−26] Recently, it was demonstrated that in ba_3 the Cu_B−His environment is very rigid and not subject to conformational transitions that are associated with protonation/deprotonation events of the Cu_B His ligands and that the farnesyl−tyrosine linkage has no direct control on the ν(CO) stretching frequency and, thus, on the type (α or β) of the stable conformation that is present in heme−copper oxidases.[26] In addition, it has been

* To whom correspondence should be addressed. E-mail: varotsis@edu.uoc.gr. Fax: +30-2810-545001. Phone: +30-2810-545053.
[†] University of Crete.
[‡] University of Cyprus.

10.1021/jp0718597 CCC: $37.00
Published on Web 08/14/2007

demonstrated that the role of the cross-linked tyrosine is to fix Cu_B in a certain configuration and distance from heme a_3.[12] The *cbb*$_3$ enzyme isolated from *Pseudomonas stutzeri* contains three *c*-type low-spin hemes, one low-spin *b*-type heme, and a heme b_3-Cu_B binuclear center.[32] In the *cbb*$_3$ oxidase, the cross-linked tyrosine is at a different location in the sequence.[31] Time-resolved step-scan FTIR (TRS^2-FTIR) has revealed that in *cbb*$_3$-type oxidase the decay of the transient Cu_B-CO complex, in contrast to *aa*$_3$, is concurrent with the formation of the heme b_3-CO complex and that the ν(CO) of Cu_B is located at 2065 cm^{-1}, despite the lack of the hydroxyethylfarnesyl side chain, similar to that observed in cytochrome *aa*$_3$ and cytochrome *bo*$_3$.[25]

There are conflicting reports in the literature regarding the properties of the Cu_B ligands and their role in the formation of the heme Fe−CO vibrations (α-, β-, and γ-forms).[14−21,23] In an effort to clarify these differences and to further explore the dynamics of the environment of Cu_B we have investigated the pH-dependent changes in the heme−copper binuclear site of the CO derivative of *cbb*$_3$ by TRS^2-FTIR. We have also used density functional theory to investigate the dynamics of the environment of Cu_B upon ligand detachment and/or deprotonation of its His ligands including the cross-linked tyrosine. Our combined FTIR data and DFT calculations indicate that the Cu_B-His ligands including the cross-linked tyrosine are affected by the protein environment but without any changes in their protonation and coordination properties in the pH/pD 7−9 range. Consequently, we exclude the involvement of Cu_B ligands, in contrast to previous reports, as crucial elements in the function of heme−copper oxidases. Our data also indicate that the contribution of Cu_B to the split of the heme Fe−CO vibrations (α-, β-, and γ-forms) is not the result of changes in the ligation and or protonation states of its ligands but rather to a global protein conformational change in the vicinity of Cu_B that affects the distance between the two metal centers.

Experimental Methods

The purification of *cbb*$_3$ oxidase was according to a previously published procedure.[25] Dithionite-reduced samples were exposed to 1 atm of CO (1 mM) in an anaerobic cell to prepare the carbonmonoxy adduct and loaded anaerobically into a cell with CaF_2 windows. CO gas was obtained from Messer (Germany). FTIR spectra were obtained from 400−500 μM samples with a Bruker Equinox 55 FTIR spectrometer equipped with liquid nitrogen cooled mercury cadmium telluride (MCT) detector. The 355 nm pulses from a Continuum Nd:YAG laser (7 ns width, 3−7 Hz) were used as a pump light (3−4 mJ/pulse) to photolyze the *cbb*$_3-$CO oxidase for the time-resolved step-scan experiments. In these experiments, a TTL pulse (transistor transistor logic) provided by a digital delay pulse generator (Quantum Composers, 9314T) triggers the flashlamps, Q-switch, and the FTIR spectrometer. Pretriggering the FTIR spectrometer to begin data collection before the laser fires allows 11 fixed reference points to be collected at each mirror position, which are used as the reference spectrum in the calculation of the difference spectra. Changes in intensity were recorded with an MCT detector (Graseby Infrared D316, response limit 600 cm^{-1}) amplified in the dc-coupled mode and digitized with a 200 kHz, 16-bit, analog-to-digital converter. A broad-band interference optical filter (Optical Coating Laboratory, Santa Rosa, CA) with short wavelength cutoff at 2.67 μm was used to limit the free spectral range from 2.67 to 8 μm. This leads to a spectral range of 3900 cm^{-1}, which is equal to an undersampling ratio of 4. Single-sided spectra were collected at 8 cm^{-1} spectral resolution, 5 μs time resolution, 10 coadditions per data point. Total accumulation time for each measurement was 60 min, and 2−3 measurements were collected and averaged. Blackman−Harris three-term apodization with 32 cm^{-1} phase resolution and the Mertz phase correction algorithm were used. Difference spectra were calculated as $\Delta A = -\log(I_S/I_R)$. Optical absorption spectra were recorded with a Perkin-Elmer Lamda 20 UV−vis spectrometer before and after the FTIR measurements to ensure the formation and stability of the CO adducts.

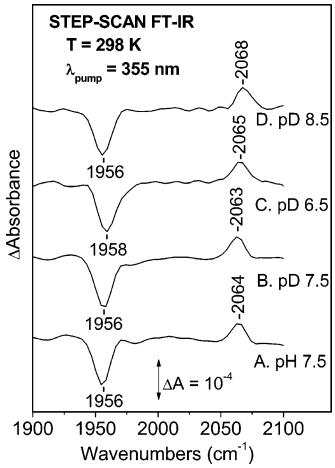

Figure 1. Step-scan time-resolved FTIR (TRS^2-FTIR) difference spectra of the CO-bound form of fully reduced cytochrome *cbb*$_3$ oxidase, at the indicated pH and pD values, 10 μs after CO photolysis from heme *a*$_3$. The path length was 15 and 30 μm for the pH and pD samples, respectively, the spectral resolution was 8 cm^{-1}, the time resolution was 5 μs, and 10 coadditions were collected and averaged per data point. The excitation wavelength was 355 nm (4 mJ/pulse), and three measurements were recorded and averaged for each data set. The spectra are normalized to the intensity of the 2065 cm^{-1} mode.

Density Functional Theory. We have designed four groups of models, referring to them as **A**, **B**, **C** (Figure 2), and **D** (Figure 3). In these models, Cu_B (I) is coordinated to three (**A1**−**A4**) and two (**A5**) imidazoles and the cross-linked His-Tyr is designed as a cross-linked imidazole−phenol (protonated) unit. In **A2**−**A4** the phenol is deprotonated. In **A3** and **A4** the phenolic O is H-bonded to H_3O^+ and H_2O, respectively. In group **B**, the imidazoles coordinated to Cu_B in group **A** are substituted by NH_3 ligands, while the cross-link Im−phenol unit remains protonated in **B1** and deprotonated in **B2** and **B3**; in **B3** the phenolic O is H-bonded to H_3O^+. **B4** is similar to **B1** but with one instead of two coordinated NH_3 ligands. **B5** lacks both NH_3 ligands of **B1**. In **C1** and **C2**, Cu_B is coordinated to three imidazoles without the cross-linked phenol unit. In **C1**, all imidazoles are protonated, and in **C2** one of the three imidazoles is deprotonated. In **C3**, Cu is coordinated to two protonated imidazoles. In **C4**, Cu is coordinated to a deprotonated cross-linked Im−phenol unit. In group **D**, we have optimized structures of the binuclear $Cu_B(I)-Fe(II)$ center in which a $CH_3CH(OH)-$ group represents the hydroxyethylgeranylgeranyl or hydroxyethylfarnesyl side chain of the hemes (**D1** and **D2**) or is absent (**D3**). The distance between Cu(I) and Fe(II) is constrained to ∼4.4 Å. Without this restriction in geometry, the CO-bound binuclear models converge to structures where metals drift apart (7−8 Å) resulting to an unusually open binuclear cavity. In Figure 2 the HOMO of **A1** and **A2** are also presented.

DFT calculations are performed on systems with $Cu_B(I)$ and heme−Fe(II) leading to a *singlet*, positively charged (+1) mononuclear $Cu_B(I)-CO$ complex or a binuclear $Cu_B(I)-CO$ Fe(II) center. For each structure considered, a full geometry

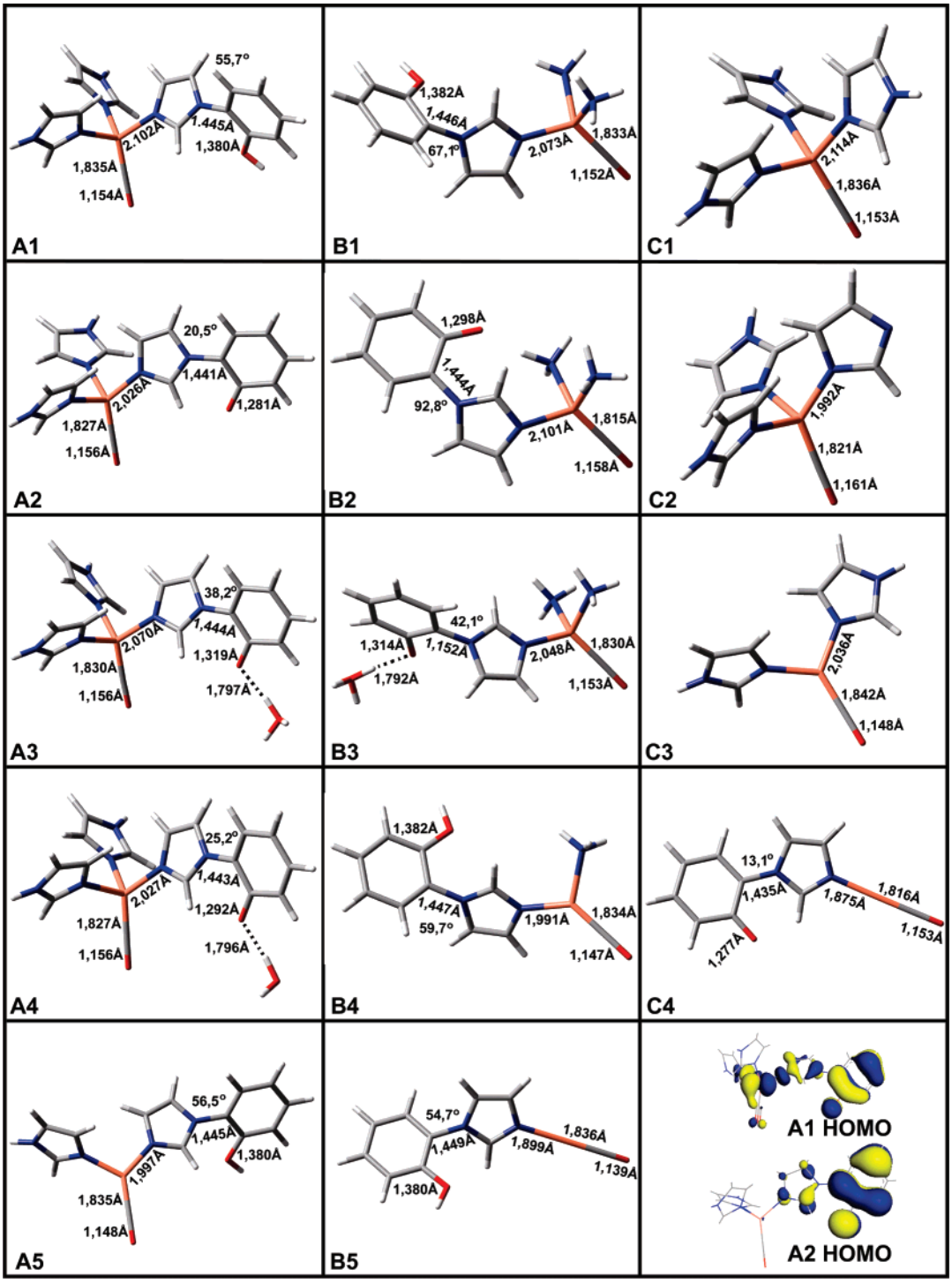

Figure 2. Geometry-optimized models of the Cu_B active site in different ligand protonation or dissociation states. Selected distances of O−C, C−Cu, Cu−N, cross-link N−C, and (phenol) C−O are also shown in angstroms. The imidazole−phenol torsion angle appears in degrees.

optimization was performed using the density functional BLYP method of the dmol3 module in Accelrys Materials Studio 2.21.[35−37] Double-numerical plus d-functions with a polarization d-function on all non-hydrogen atoms are used for all light elements. For the metals (iron and copper) the effective core potential (ECP) from the Stuttgart−Dresden group was used as this is implemented in the dmol3 module of Materials Studio (Accelrys).[38,39] The functional GGA/BLYP on a DND basis set used for the calculations is consistent with a BLYP/6-31G(d) level calculation in Gaussian software package. In all cases (convergence tolerance, integration accuracy, SCF tolerance) level fine was selected.

Results

Figure 1 shows the TRS^2-FTIR difference spectra (t_d = 10 μs, 8 cm^{-1} spectral resolution) of fully reduced *cbb*$_3$−CO subsequent to CO photolysis by a nanosecond laser pulse (355 nm) at pH 7.5 and in the pD 6.6−8.5 range. Upon photolysis, CO is transferred from heme b_3 to Cu_B. In Figure 1A, the negative peak at 1956 cm^{-1} arises from the photolyzed heme b_3^{2+}−CO complex and the positive peak that appears at 2064 cm^{-1} (t_d = 10 μs) is attributed to the C−O stretch (ν_{CO}) of the transient Cu_B^{1+}−CO complex. The frequencies and bandwidths

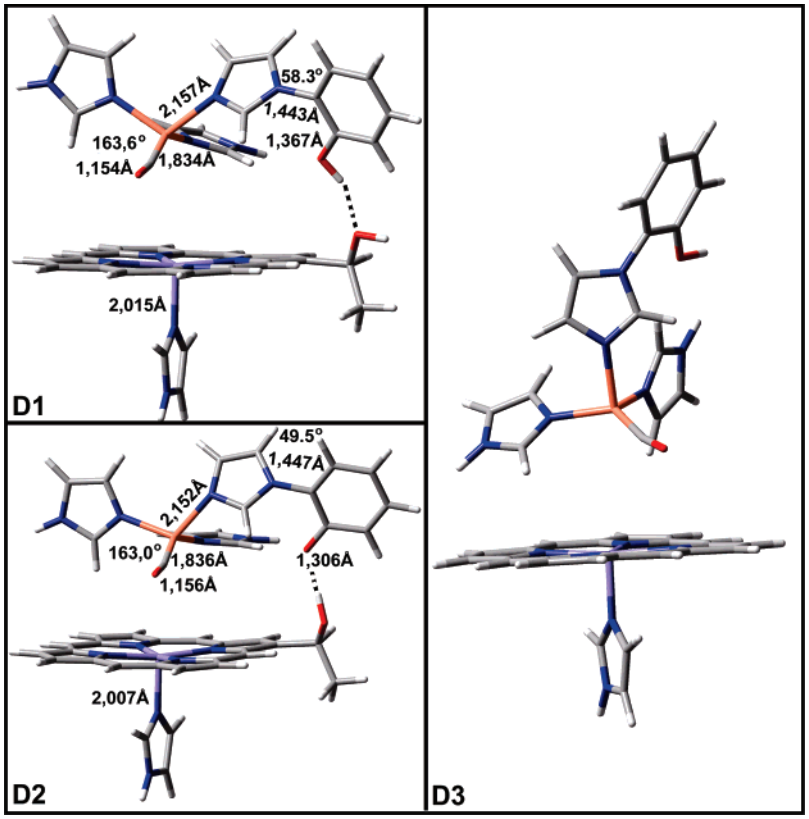

Figure 3. (D1 and D2) Geometry-optimized structures of the binuclear center while CO is bound on the Cu_B site show the effect on bending/tilting for the −C≡O ligand due to the porphyrin molecule and cross-linked phenol deprotonation. Distances of bonds like O−C, C−Cu, Cu−N, cross-link N−C, (phenol) C−O, and Im−Fe are shown in black. Bending of Cu−C−O moiety is shown in degrees, as well as the imidazole−phenol torsion angle. (D3) The unusual position of the phenol unit cross-linked to the imidazole ligand shows the effect of no interaction between the copper and iron sites.

TABLE 1: Cu−C−O Vibrational Frequencies

Cu_B−CO models	theor frequencies (cm^{-1}) (dmol3-BLYP/DND) ν(C−O)	ν(Cu−C)/δ(Cu−C−O)	exptl ν(C−O)
A1	**2031**	**414/326**	(α-form Cu_B)
A2	2020	425	
A3	2020	420	aa_3 2065[a] (300 K)
A4	2023	421	2064[b] (10 K)
A5	2072	421	2061[c] (84, 183 K)
B1	**2049**	**419**	ba_3 2053[d] (300 K)
B2	2011	442	cbb_3 2065[e] (300 K)
B3	2040	421	
B4	2083	422	(β-form Cu_B)
B5	2147	444	
C1	**2035**	**411/324**	aa_3 2043[a] (10 K)
C2	1992	431	2039[b] (10 K),
C3	2078	411	2038[c] (84 K)
C4	2026	468	2045[c] (183 K)

[a] Bovine.[41−44] [b] *Rh. sphaeroides*.[20] [c] *P. denitrificans*.[27] [d] *T. thermophilus*.[26,42,43] [e] *P. stutzeri*.[25]

of these C−O modes remained similar between H_2O and D_2O. However, at pD 8.5, the CO frequency appeared at 2068 cm^{-1}.

Density Functional Theory. Table 1 summarizes the calculated ν(Cu−C), ν(C−O), and selected δ(Cu−C−O) frequencies for the **A**−**C** models. Table 2 summarizes the phenolic ring stretching and coupled phenol−imidazole stretching frequencies of models **A1** and **A2**.

Accuracy of the DFT Results on the blyp/dnd Level. To check the validity of dmol3 results, calculations on models with CO bound to Cu_B have been performed using Gaussian 98 software package on a higher level of theory (b3lyp/lanl2dz).[49] The calculated frequencies for the Cu−C stretching mode are 380 cm^{-1} for **A1** and 391 cm^{-1} for **A5**. Thus, we observe a +11 cm^{-1} shift in frequencies in the higher level of theory and +7 cm^{-1} for the BLYP/DND (dmol3) level. Both methods calculate a ν(CO) frequency of 2031 cm^{-1} for **A1**, whereas in **A5**, there is a 1 cm^{-1} difference for the ν(CO) frequency. Geometric parameters, such as bond lengths and angles, differ only of a maximum amount of ±0.04 Å and 5−6°, respectively, between the two levels of theory. Despite the differences in the absolute values of the vibrational frequencies between the two methods, the calculated frequency shifts follow the same trend. All frequencies have considerably large intensities, and thus, their derived shifts are experimentally observable.

The Cross-Linked His-Tyr Unit. Different imidazole−phenol torsion angles (models **A2**, **A3**, and **A4**) or the absence of the cross-linked phenol unit (models **A1** and **C1**) have no significant effect (3−4 cm^{-1}) on the ν(CO). Orientation (torsion angles) of the ligands coordinated to Cu_B is quite fixed and determined in a way by the protein matrix, whereas in our Cu_B models such orientation is not taken into account. However, this does not affect the ν(CO) and ν(Cu−C) frequencies as explained above, and thus, our DFT results are consistent with those observed experimentally for Cu_B−CO.

Changes in the Coordination of Cu_B. A close inspection of the data presented in Table 1 shows large frequency shifts in ν(CO) when Cu_B looses one of its imidazole (or NH_3 in simpler models) ligands. When a Cu_B−Im bond scission occurs, ν(CO) shifts to higher frequency by 41 cm^{-1} (**A5** compared to **A1**), as the C−O bond strengthens due to geometrical and electronic structural changes in Cu. A relatively smaller effect (7 cm^{-1}) is calculated for ν(Cu−C) in the same set of models.

TABLE 2: Cross-Linked Phenol- and Imidazole-Related Vibrational Frequencies Are Shown in the dmol3-BLYP/DND Level of Theory[a]

model	character of vibration	dmol3 BLYP/DND (this study)	experimental	
			enzyme	models
A1	phenolic ring stretching	1495	1515 (45)	1515 (46)
	phenolic ring/C−O	1238	1248 (47)	1249 (48)
	coupled phenol−imidazole and C−N cross-link	1446 1470 1583 1589	1480/1550 (46) 1546 (47)	1480/1546 (46) 1478/1548 (14)
A2	phenolic ring stretching	1481		
	phenolic ring/CO	1257		1266 (14) 1269 (48)
	coupled phenol−imidazole and C−N cross-link	1448 1493 1509 1576		

[a] Experimental results for model compounds and heme−copper oxidases are also shown for reference.

Protonation State of Copper Ligands. A change in the protonation state of one of the Cu_B imidazole ligands (comparison of **C1** to **C2**) has significant change in the back-donation of electron density and therefore the vibrational frequencies with a calculated shift of 20−43 cm^{-1}, whereas deprotonation of the phenol unit (comparison **A1** to **A2**) strengthens the Cu−C and weakens the C−O bond leading to a frequency shift of 11 cm^{-1}. In the case where Cu lacks two of the three imidazoles (**C4**) or the two imidazoles are replaced by NH_3 groups, the deprotonation of the cross-linked phenol unit (**B5** → **C4** or **B1** → **B2**) has a pronounced effect of 121 cm^{-1} and 38 cm^{-1}, respectively. The calculated frequencies indicate that electron density due to phenol deprotonation moves mainly to the Cu−C−O entity, altering bond lengths and vibrational frequencies. On the other hand, if Cu is coordinated to three imidazoles (structures **A1**, **A2**), electron density due to phenol deprotonation does not localize to the Cu−C−O moiety but rather is delocalized on the whole Cu_B complex, including the histidine ligands, leading to a reduced $\Delta\nu$(CO) effect of 11 cm^{-1}.

Binuclear Models. The results show certain aspects of the coordination properties of Cu_B that can either support or reject proposed mechanisms based on experimental data. Differences in the vibrational properties between experiment and theory can be partly attributed to the absence of the heme Fe in our models (**A**, **B**, and **C**), which would alter the −C≡O bending and tilting. Figure 3 shows geometry-optimized binuclear models containing both Cu_B and heme Fe. Models **A**, **B**, and **C** exhibit an almost linear Cu−C−O geometry compared to **D1** and **D2**, where the Cu−C−O tilt and bending is different when the heme Fe is present but remains unaltered in deprotonation events. Therefore, the calculated frequency differences on deprotonation or ligand dissociation are not affected by the presence of the heme Fe.

Models **D1** and **D2** were altered in such way that CO is bound to heme−iron rather than to copper (structures not shown). Geometry optimization was performed on the same blyp/dnd (dmol3) level of theory. CO geometry (bending or tilting) is affected as the distance between the metal sites changes. Iron−copper distance was kept constant at 6.0, 5.0, and 4.5 Å for the above models, and the rest of the active site was left free to be optimized. Tilt/bend of the Fe−C−O moiety was calculated to be 87.9°/178.0° (6.0 Å), 84.7°/173.9° (5.0 Å), and 80.5°/169.1° (4.5 Å).

Discussion

DFT Calculations. In the Cu_B−CO models the changes in the bond lengths of the bound CO and, thus the calculated frequency shifts, can be attributed to the increase of electron density on the metal center: as the electron density on the metal center increases (deprotonation increases the flow of electron density to Cu_B as discussed above) more electron density donation to the CO ligand takes place. This increases the M−CO bond strength making it more double-bond-like (M═C═O) which in turn, further weakens the C−O bond by increasing the electron density into the carbonyl antibonding orbitals. Trans ligands to a carbonyl can have a particularly large effect on the ability of the CO ligand to effectively π-back-bond to the metal. For example, two trans π-back-bonding ligands will partially compete for the same d-orbital electron density, weakening each other's net π-back-bonding. Trans ligands which are σ-donors can increase the M−CO bond strength (more M═C═O character) by allowing unimpeded metal-to-CO π-back-bonding.

Different bond lengths and dihedral angles between the phenol and imidazole planes are reported in the literature for the C−N cross-link.[14−18] In our models, the calculated C−N length is 1.4−1.5 Å and is fully consistent with that experimentally observed (1.427 Å) and theoretically calculated (1.40−1.44 Å in b3lyp/6-31g* level of theory) by Nagano and co-workers.[17,18] In the case of **A1** and **A2** the dihedral angles are calculated to be 55.7° and 20.5°, respectively, indicating that π-conjugation between the two rings is much larger in the case of the deprotonated phenol unit (**A2**) and remains unchanged in the cases of **A1**, **A5**, and **B5** where the copper ligands are two in **A5** and one in **B5**. Therefore, ligand dissociation does not affect the π-conjugation between the two parts of the cross-link system, as dihedral angles are almost the same. The calculated Cu−N bond lengths are in the range of 1.9−2.1 Å and remained unchanged when deprotonation or ligand dissociation in the coordination sphere of Cu takes place.

The normal modes presented in Table 2 correspond mainly to a mixture of phenol−imidazole modes.[17,18,50] Nagano and co-workers have suggested that the imidazole−phenol cross-linkage causes only a minor modification to the electronic structure of the ground state of their model compound and that the cross-linked tyrosine sustains its protonated state unless proton transfer is coupled to electron transport.[17,18] On the other hand, a few groups have proposed that the histidine−tyrosine

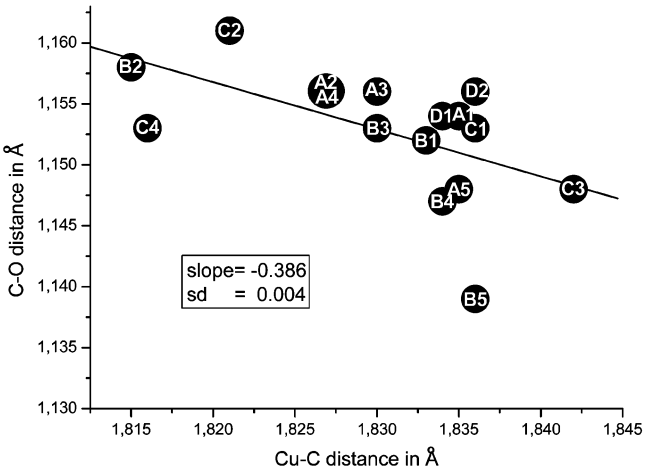

Figure 4. Negative slope in the d(C−O) vs d(Cu−C) diagram implies the presence of π-back-bonding in Cu−CO complexes. The above distances correspond to models in groups A, B, C, and D.

cross-link may facilitate proton delivery to the active heme Fe site of CcO in the catalytic cycle.[14−16,51] The present study indicates that the absence of the cross-linked phenol unit (comparison of models **A1** and **C1**) has a minor effect on the vibrational frequencies of the Cu−C−O unit. On the other hand, deprotonation of the cross-linked tyrosine affects the frequency of the CO bound to Cu_B. Because the pK_a of the phenolic hydroxyl is ca.10 in the ground state, which is similar to that of the *p*-cresol (tyrosine), we suggest that any pH dependency of the Cu_B−C−O vibrational frequencies in heme−copper oxidase is not due to deprotonation of the cross-linked tyrosine.[18]

It has been generally believed that the ligands of Cu_B are critically involved in the catalytic and proton-pumping function of CcO owing to their close proximity to the heme a_3 center.[52−58] A histidine cycle,[54] a histidine cycle/shuttle[55] as well as the protonated/deprotonated state of His290[56] have been proposed as the crucial elements in the proton-pumping pathway and the cross-linked tyrosine as the electron donor[58] for the formation of the P intermediate. The existence and identity of such reorganization of the Cu_B geometry caused by protonation/deprotonation and/or breakage of one of the Cu−N(His) bonds has been a difficult matter to either prove or disprove since Cu_B is spectrally silent, and therefore no definite spectroscopic evidence had been observed.

The ν(CO) frequency of the transient Cu_B−CO complex determines in great amount the conformational changes (e.g., ligand dissociation) of the copper metal site in CcO, whereas both ν(CO) and ν(Cu−C) are reliable criteria for protonation/deprotonation phenomena. Therefore, we can derive structural information for the Cu_B His ligands from the ν(CO) frequency of the Cu_B^{1+}−CO complex. The negative slope in the diagram of the DFT-optimized distances, d(C−O) versus d(Cu−C), implies the presence of a π-back-bonding in the Cu−CO complexes (Figure 4). The calculated ν(CO) frequencies of Cu_B under different protonation/deprotonation states and/or ligand detachment indicate that the ν(CO) frequency depends strongly on the degree of back-bonding. A change in the protonation state of one of the His ligands would have significant changes in the back-donation and, thus, on the frequency of ν(CO). The small variation (3−4 cm^{-1}) of the ν(CO) of Cu_B as compared with that predicted from the DFT calculations indicates that the degree of back-donation of electron density from the d orbitals to the antibonding π^* orbitals is not significantly altered under these conditions. Similar results have been reported for ba_3.[26] If one of the His ligands of Cu_B is

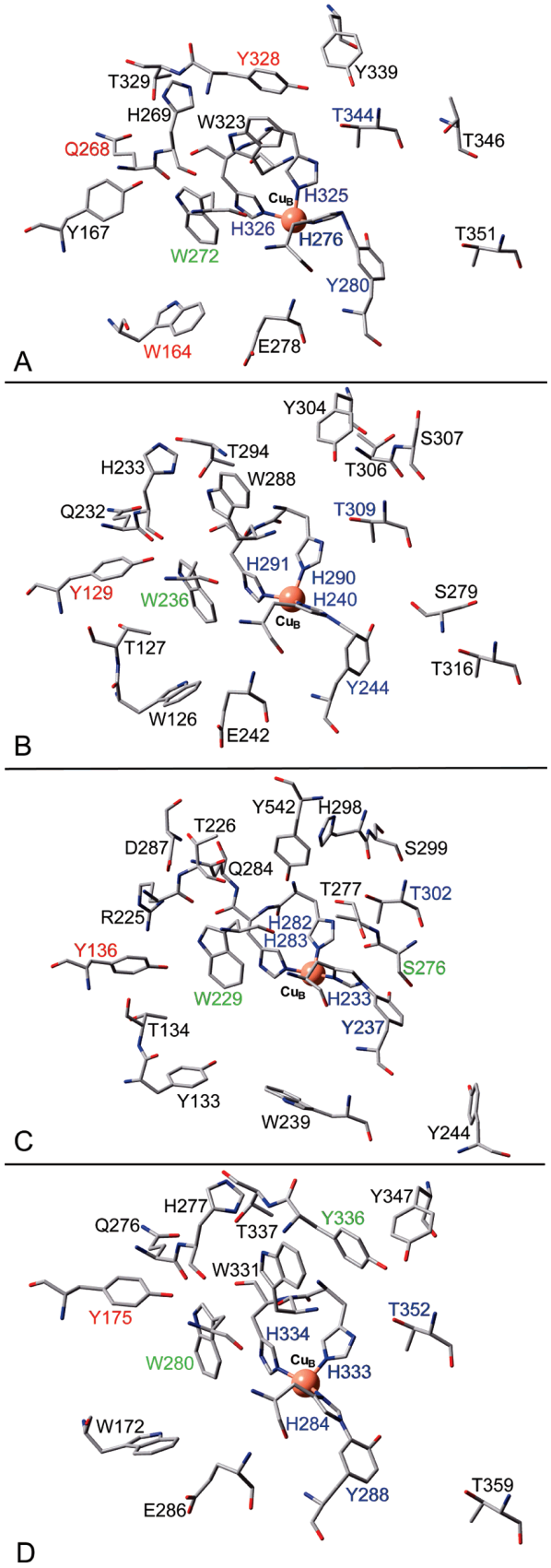

Figure 5. Residues near the Cu_B site in (A) aa_3 from *P. denitrificans*, (B) *bovine*, (C) ba_3 from *T. thermophilus*, and (D) aa_3 from *Rh. sphaeroides*. Different coloring of residue names is used to mark the distance from the amino acids to Cu_B. Blue marks a distance of close to or less than 3 Å; green, a distance of around 5 Å; red, a distance between 6 and 7 Å; black, labels a distance in the 7−10 Å range.

capable of cycling through the imidazolate, imidazole, and imidazolium states then ν(CO) is expected to vary. Therefore, no structural change at Cu_B occurs in association with CO binding to and dissociation from heme a_3. This observation in conjunction with the above conclusion that the pH/pD dependency of the Cu_B-C-O vibrational frequencies in heme−copper oxidase is not due to deprotonation of the cross-linked tyrosine demonstrates that the environment of Cu_B does not serve as a proton-labile site.

In geometry-optimized heme Fe− Cu models, the cross-linked phenol unit plays a crucial role in stabilizing the $Fe-Cu_B$ distance, as it interacts with *hydroxyethylfarnesyl* or *hydroxyethylgeranylgeranyl* side chain of the porphyrin. Models lacking such porphyrin side chain (cbb_3) converge to DFT structures in which the $Fe-Cu_B$ distance or the ligation geometry of Cu_B are not consistent to the crystal structures. One of such models, **D3**, where the phenol unit drifts away from the porphyrin, converges to an unusual active site structure. Theoretical models like **D3** are consistent with a more open active site cavity like in cbb_3 oxidase, in which the *hydroxyethylfarnesyl* side chain is absent.

Conclusions

Conformations of the Heme $Fe-Cu_B$ Binuclear Center. The data presented here and those previously reported suggest that between pH 7 and 9 the chemical environment does not alter the protonation state of the Cu_B histidine ligands and the cross-linked tyrosine.[10,12,19−27,59] Consequently, the contribution of Cu_B to the split of the CO vibrations (α-, β-, and γ-forms) is the result of a more global protein conformational change in the vicinity of Cu_B that affects its position with respect to the heme Fe and not due to changes in the ligation and/or protonation states of the Cu_B ligands. Figure 5 compares the structures of the Cu_B environment of four heme−copper oxidases isolated from different sources. Although the Cu_B ligands are highly conserved among the four different heme−copper oxidases, the behavior of the α-, β-, and γ-forms of the CO bound to the heme Fe and their pH behavior are quite different. We suggest that protonation/deprotonation of amino acid residues in the vicinity of Cu_B with pK_a in the 7−9 range, which are not conserved among the heme−copper oxidases, affects the position of Cu_B with respect to the heme Fe, creating the experimentally observed α-, β-, and γ-forms of the CO bound to the heme Fe. Furthermore, the role of the cross-link is to fix Cu_B in a certain configuration and distance from the heme Fe through its interaction with the *hydroxyethylfarnesyl* chain and, thus, producing the above-mentioned forms of the CO bound to the heme Fe.[12]

References and Notes

(1) Wikström, M. *Nature* **1989**, *338*, 776.
(2) Ferguson-Miller, S.; Babcock, G. T. *Chem. Rev.* **1996**, *96*, 2889.
(3) Gennis, R. B. *Biochim. Biophys. Acta* **1998**, *1365*, 241.
(4) Michel, H. *Proc. Natl. Acad. Sci. U.S.A.* **1998**, *95*, 12819.
(5) Trumpower, B. L.; Gennis, R. B. *Annu. Rev. Biochem.* **1994**, *63*, 675.
(6) Babcock, G. T.; Wikström, M. *Nature* **1992**, *356*, 301.
(7) Tsukihara, T.; Aoyama, H.; Yamashita, E.; Tomizaki, T.; Yamaguchi, H.; Shinzawa-Itoh, K.; Nakashima, R.; Yaono, R.; Yoshikawa, S. *Science* **1995**, *269*, 1069.
(8) Iwata, S.; Ostermeier, C.; Ludwig, B.; Michel, H. *Nature* **1995**, *376*, 660.
(9) Soulimane, T.; Buse, G.; Bourenkov, G. P.; Bartunik, H. D.; Huber, R.; Than, M. E. *EMBO J.* **2000**, *19*, 1766.
(10) Das, T. K.; Pecoraro, C.; Tomson, F. L.; Gennis, R. B.; Rousseau, D. L. *Biochemistry* **1998**, *37*, 14471.
(11) Proshlyakov, D. A.; Pressler, M. A.; Babcock, G. T. *Proc. Natl. Acad. Sci. U.S.A.* **1998**, *95*, 8020.
(12) Pinakoulaki, E.; Pfitzner, U.; Ludwig, B.; Varotsis C. *J. Biol. Chem.* **2002**, *277*, 13563.
(13) Pinakoulaki, E.; Pfitzner, U.; Ludwig, B.; Varotsis, C. *J. Biol. Chem.* **2003**, *278*, 18761.
(14) Cappucio, J. A.; Ayala, I.; Elliot, G. I.; Szundi, I.; Lewis, J.; Konopelski, J. P.; Berry, B. A.; Einarsdótirr, O. *J. Am. Chem. Soc.* **2002**, *124*, 1750.
(15) Berry, B. A.; Einarsdótirr, O. *J. Phys. Chem. B* **2005**, *109*, 6972.
(16) McCauley, K. M.; Vrtis, J. M.; Dupont, J.; van der Donk, W. A. *J. Am. Chem. Soc.* **2000**, *122*, 2403.
(17) Nagano, Y.; Liu, J-G.; Naruta, Y.; Kitagawa, T. *J. Mol. Struct.* **2005**, *736*, 279.
(18) Nagano, Y.; Liu, J-G.; Naruta, Y.; Ikoma, T.; Tero-Kubota, S.; Kitagawa, T. *J. Am. Chem. Soc.* **2006**, *128*, 14560.
(19) Das, T. K.; Tomson, F. K.; Gennis, R. B.; Gordon, M.; Rousseau, D. L. *Biophys. J.* **2001**, *80*, 2039.
(20) Mitchell, D. M.; Shapleigh, J. P.; Archer, A. M.; Alben, J. O.; Gennis, R. B. *Biochemistry* **1996**, *35*, 9446.
(21) Wang, J.; Takahashi, S.; Hosler, P. H.; Mitchell, D. M.; Ferguson-Miller, S.; Gennis, R. B.; Rousseau, D. L. *Biochemistry* **1995**, *34*, 9819.
(22) Varotsis, C.; Vamvouka, M. *J. Phys. Chem. B* **1998**, *102*, 7670.
(23) Hosler, P. H.; Kim, Y.; Shapleigh, J. P.; Gennis, R. B.; Alben, J. O.; Ferguson-Miller, S.; Babcock, G. T. *J. Am. Chem. Soc.* **1994**, *116*, 5515.
(24) Pinakoulaki, E.; Soulimane, T.; Varotsis, C. *J. Biol. Chem.* **2002**, *277*, 32867.
(25) Stavrakis, S.; Koutsoupakis, K.; Pinakoulaki, E.; Urbani, A.; Saraste, M.; Varotsis, C. *J. Am. Chem. Soc.* **2002**, *124*, 3814.
(26) Koutsoupakis, K.; Stavrakis, S.; Soulimane, T.; Varotsis, C. *J. Biol. Chem.* **2003**, *278*, 14893.
(27) Rost, B.; Behr, J.; Hellwig, P.; Richter, O.-M. H.; Ludwig, B.; Michel, H.; Mäntele, W. *Biochemistry* **1998**, *38*, 7565.
(28) Pinakoulaki, E.; Ohta, T.; Soulimane, T.; Kitagawa, T.; Varotsis, C. *J. Biol. Chem.* **2004**, *279*, 22791.
(29) Ohta, T.; Pinakoulaki, E.; Soulimane, T.; Kitagawa, T.; Varotsis, C. *J. Phys. Chem. B* **2004**, *108*, 5489.
(30) Varotsis, C.; Babcock, G. T.; Garcia-Horsman, A.; Gennis, R. B. *J. Phys. Chem.* **1995**, *99*, 16817.
(31) Hemp, J.; Christian, C.; Barquera, B.; Gennis, R. B.; Martinez, T. J. *Biochemistry* **2005**, *44*, 10766.
(32) Urbani, A.; Gemeinhardt, S.; Warne, A.; Saraste, M. *FEBS Lett.* **2001**, *508*, 29.
(33) Giuffrè, A.; Stubauer, G.; Sart, P.; Brunori, M.; Zumft, W. G.; Buse, G.; Soulimane, T. *Proc. Natl. Acad. Sci. U.S.A* **1999**, *96*, 14718.
(34) Pinakoulaki, E.; Ohta, T.; Soulimane, T.; Kitagawa, T.; Varotsis, C. *J. Am. Chem. Soc.* **2005**, *127*, 15161.
(35) Dmol3 module of *Cerius*^{2}; Accelrys: San Diego, CA, 1999.
(36) Delley, B. J. *J. Chem. Phys.* **1990**, *92*, 508.
(37) Accelrys-Materials Studio, Quantum and Catalyses Tools, DMol3, March 1, 2005. http://www.accelrys.com/mstudio/ms-modeling/dmol3.html.
(38) Dolg, M.; Wedig, U.; Stoll, H.; Preuss, H. *J. Chem. Phys.* **1987**, *86*, 866.
(39) Bergner, A.; Dolg, M.; Kuechle, W.; Stoll, H.; Preuss, H. *Mol. Phys.* **1993**, *80*, 1431.
(40) Koutsoupakis, C.; Soulimane, T.; Varotsis, C. *Biophys. J.* **2004**, *86*, 2438.
(41) Park, S.; Pan, L.-P.; Chan, S. I.; Alben, J. *Biophys. J.* **1996**, *71*, 1036.
(42) Woodruff, W. H. *J. Bioenerg. Biomembr.* **1993**, *25*, 177.
(43) Einarsdótirr, Ó.; Killough, P. M.; Fee, J. A.; Woodruff, W. H. *J. Biol. Chem.* **1989**, *264*, 2405.
(44) Einarsdótirr, Ó.; Dyer, R. B.; Lemon, D. D.; Killough, P. M.; Hubig, S. M.; Atherton, S. J.; Lopez-Garriga, J. J.; Palmer, G.; Woodruff, W. H. *Biochemistry* **1993**, *32*, 12013.
(45) McMahon, B. H.; Fabian, M.; Tomson, F.; Causgrove, T. P.; Bailey, J. A.; Rein, F. N.; Dyer, R. B.; Palmer, G.; Gennis, R. B.; Woodruff, W. H. *Biochim. Biophys. Acta* **2004**, *1655*, 321.
(46) Tomson, F.; Bailey, J. A.; Gennis, R. B.; Unkefer, C. J.; Zizhong, L.; Silks, L. A.; Martinez, R. A.; Donohoe, R. J.; Dyer, R. B.; Woodruff, W. H. *Biochemistry* **2002**, *41*, 14383.
(47) Nyquist, R. M.; Heitbrink, D.; Bolwien, C.; Gennis, R. B.; Heberle, J. *Proc. Natl. Acad. Sci. U.S.A.* **2003**, *100*, 8715.
(48) Hellwig, P.; Pfitzner, U.; Behr, J.; Rost, B.; Pesavento, R. P.; van der Donk, W. A.; Gennis, R. B.; Mitchel, H.; Ludwig, B.; Mäntele, W. *Biochemistry* **2002**, *41*, 9116.
(49) Frisch, M. J.; Trucks, G. W.; Schlegel, H. B.; Scuseria, G. E.; Robb, M. A.; Cheeseman, J. R.; Zakrzewski, V. G.; Montgomery, J. A., Jr.; Stratmann, R. E.; Burant, J. C.; Dapprich, S.; Millam, J. M.; Daniels, A. D.; Kudin, K. N.; Strain, M. C.; Farkas, O.; Tomasi, J.; Barone, V.; Cossi, M.; Cammi, R.; Mennucci, B.; Pomelli, C.; Adamo, C.; Clifford, S.; Ochterski, J.; Petersson, G. A.; Ayala, P. Y.; Cui, Q.; Morokuma, K.; Salvador, P.; Dannenberg, J. J.; Malick, D. K.; Rabuck, A. D.; Raghavachari, K.; Foresman, J. B.; Cioslowski, J.; Ortiz, J. V.; Baboul, A. G.; Stefanov, B. B.; Liu, G.; Liashenko, A.; Piskorz, P.; Komaromi, I.; Gomperts, R.;

Martin, R. L.; Fox, D. J.; Keith, T.; Al-Laham, M. A.; Peng, C. Y.; Nanayakkara, A.; Challacombe, M.; Gill, P. M. W.; Johnson, B.; Chen, W.; Wong, M. W.; Andres, J. L.; Gonzalez, C.; Head-Gordon, M.; Replogle, E. S.; Pople, J. A. *Gaussian 98*, revision A.11; Gaussian Inc.: Pittsburgh, PA, 2001.

(50) Aki, M.; Ogura, T.; Naruta, Y.; Le, T. H.; Kitagawa, T. *J. Phys. Chem. A* **2002**, *106*, 3436.

(51) Collman, J. P.; Wang, Z.; Zhong, M.; Zeng, L. *J. Chem. Soc., Perkin Trans.* **2000**, *11*, 1217.

(52) Himo, F.; Noodleman, L.; Blomberg, M. R. A.; Siegbahn, P. E. M. *J. Phys. Chem. A* **2002**, *106*, 8757.

(53) Liu, J. G.; Naruta, Y.; Tani, F. *Angew. Chem., Int. Ed.* **2005**, *44*, 1836.

(54) Morgan, J. E.; Verkhovsky, M. I.; Wikström, M. *J. Bioenerg. Biomembr*. **1994**, *26*, 599.

(55) MacMillan, F.; Kannt, A.; Behr, J.; Prisner, T.; Michel, H. *Biochemistry* **1999**, *38*, 9179.

(56) Das, T. K.; Gomes, C. M.; Teixeira, M.; Rousseau, D. L. *Proc. Natl. Acad. Sci. U.S.A.* **1999**, *96*, 9591.

(57) Proshlyakov, D. A.; Pressler, M. A.; DeMaso, C.; Leykam, J. F.; DeWitt, D. L.; Babcock, G. T. *Science* **2000**, *290*, 1588.

(58) Puustinen, A.; Wikström, M. *Proc. Natl. Acad. Sci. U.S.A.* **1999**, *96*, 35−37.

(59) Iwase, T.; Varotsis, C.; Shinzawa-Itoh, K.; Yoshikawa, S.; Kitagawa, T. *J. Am. Chem. Soc*. **1999**, *121*, 1415.